ELSEVIER

Chemical Physics 233 (1998) 217–229

Chemical Physics

Fifth-order two-dimensional vibrational spectroscopy of a Morse potential system in condensed phases

Yoshitaka Tanimura

Institute for Molecular Science, Myodaiji, Okazaki, Aichi 444-8585, Japan

Received 20 October 1997

Abstract

The nonlinear optical response of a molecular system in the condensed phase subjected to a series of five off-resonant femtosecond laser pulses has been studied using a quantum Fokker–Planck equation. This equation can treat a molecular system with any shape of potential coupled to a Gaussian–white noise-bath. The third- and fifth-order response functions, which are equivalent to the second- and third-order correlation functions of the molecular coordinate were obtained from the equation of motion. Assuming the potential surface of a cesium dimer [Cs_2], which is modeled by a Morse potential, and considering both the linear and nonlinear coordinate dependence of the polarizability, we calculated the third- and fifth-order response functions for various temperatures and heat-bath couplings. The temporally two-dimensional (2D) profiles of the fifth-order signal are affected by both the shape of potential and the coordinate dependence of the polarizability, even at strong damping. The nonlinearities caused by the anharmonic potential and by the nonlinear polarizability have different temperature dependence. This indicates that fifth-order two-dimensional spectroscopy carried out for a different temperature allows us to access information of the potential and the polarizability.

1. Introduction

Recent advances in femtosecond laser technology have lead us to develop higher than third-order spectroscopy such as the fifth-order [1] and seventh-order [2] off-resonant experiments. Fifth-order two-dimensional vibrational spectroscopy (two-dimensional Raman spectroscopy) has been proposed to experimentally separate the inhomogeneous distribution of slowly varying parameters, for example of local liquid configurations, from the total spectral density. This experiment uses two pairs of excitation pulses, followed by a probe pulse and therefore has two time variables. By plotting the fifth-order signal as function of these decay times, we obtain the two-dimensional profile of signal. This profile is very sensitive for the underlying nuclear dynamics and several experimental and theoretical studies have been carried out [3–13]. The fifth-order frequency-domain experiment has also been proposed [14].

Although the 2D Raman experiment was proposed to study inhomogeneity, the same technique can be used to access various dynamical information of molecules in condensed phases, such as the anharmonicity of vibrational modes [10] and the coupling mechanism between different vibration modes [8,11]. In this paper, we explore the possibility to use this technique to determine the shape of the potential and the coordinate dependence of polarizability.

In third-order off-resonant experiments, such as ISS and OKE, the signal is related to the two-time correlation function of the nuclear polarizability, $R^{(3)}(t) = \langle[\alpha(t), \alpha(0)]\rangle$, where $\alpha(t)$ is the polarizability in the Heisenberg representation. In such

0301-0104/98/$19.00
PII: S0301-0104(98)00010-X

polarizability sensitive measurements, the coordinate dependence of α is essential, since, if α is a c-number, $\alpha(t)$ commutes with $\alpha(0)$ and $R^{(3)}$ vanishes. If one expands the polarizability in terms of the nuclear coordinate denoted by Q, i.e., $\alpha = \alpha_0 + \alpha_1 Q + \alpha_2 Q^2 + \ldots$, then $R^{(3)}(t) \approx \alpha_1^2 \langle [Q(t), Q(0)] \rangle$. In the fifth-order off-resonant measurements, the signal is related to the three-time correlation function, $R^{(5)}(t,t') = \langle [[\alpha(t+t'), \alpha(t')], \alpha(0)] \rangle$. If the potential is harmonic, then the lowest order term $\alpha_1^3 \langle [[Q(t+t'), Q(t')], Q(0)] \rangle$ does not contribute to the signal, since the operator Q, which is expressed in the energy state representation as $|j\rangle\langle j \pm 1|$, cannot compose the diagonal elements, $|j\rangle\langle j|$, by the three products of Q, and the elements $\mathrm{tr}\{Q(t+t')Q(t')Q(0)|j\rangle\langle j|\}$, etc. vanish. Therefore, the leading contribution to the signal is $\alpha_1^2 \alpha_2 \langle [[Q(t+t'), Q^2(t')], Q(0)] \rangle$, etc., in which Q^2 is equivalent to $|j\rangle\langle j \pm 2|$ or $|j\rangle\langle j|$. If there is anharmonicity in the potential, however, the lowest order term is $\alpha_1^3 \langle [[Q(t+t'), Q(t')], Q(0)] \rangle$, since the Hamiltonian in the Heisenberg operator can connect the different energy state. The time- and temperature-dependence of the α_1^3 and $\alpha_1^2 \alpha_2$ terms are expected to be different, and can be used to study the anharmonicity of the potential as well as the coordinate dependence of the polarizability.

Since 2D vibrational spectroscopy is based on the analysis of the temporal profile of the signal, not of the position or the width of spectral peaks, it is important to develop a theory which can be compared with the experiments. The fifth-order theory developed so far was mainly targeting for intermolecular vibrational modes in which a Brownian oscillator model works very well. The intra-vibrational modes are, however, not necessarily harmonic. In this paper, we employ the quantum kinetic equation for reduced density matrix elements to study intra-vibrational modes, which are modeled by a system with arbitrary potential surface. In the condensed phase, a difficulty with kinetic equation approaches is the proper treatment of dephasing processes induced by the environment which serves as a heat-bath. It can be incorporated into the equation of motion, if the noise induced from the bath is Gaussian–white [15] or Gaussian–Markovian [16], in which the time correlation function of noise fluctuation, $f(t)$, can be expressed as $\langle f(t) f(t') \rangle \propto \delta(t-t')$ or $\langle f(t) f(t) \rangle \propto \exp[-\gamma(t-t')]$, respectively. In these cases, by employing the Wigner representation of the reduced density matrix, one obtains the quantum Fokker–Planck equation for a Gaussian–white noise bath [17] or a Gaussian–Markovian bath [18,19], respectively. These equations have been successfully applied to analyze femtosecond spectroscopy of nonadiabatic transitions, dissociation, predissociation and the optical Stark effect in a displaced harmonic oscillators system [20] and a displaced Morse potential system [21].

Although the Gaussian–Markovian case is more general, in this study, we limit our analysis to the Guassian–white case, since numerical calculations are much easier. The Gaussian–white noise bath we employed here has also been used in the previous study of the fifth-order spectroscopy [1,10,11]. While the previous studies are based on the path-integral approach whose applicability is limited to a harmonic system or a system with weak anharmonicity, the present Fokker–Planck approach can deal with a system with an arbitrary potential surface, but requires intensive numerical integrations.

In Section 2, we show a rigorous procedure for calculating the third- and fifth-order off-resonant response functions using the kinetic equation. The quantum Fokker–Planck equation for a Gaussian–white noise bath is given in Section 3. Model calculations for a cesium dimer [Cs_2], which is described by a Morse oscillator are presented and discussed in Section 4 for linear and nonlinear coordinate dependence of the polarizability. Section 5 is devoted to concluding remarks.

2. The third and fifth order response functions

Consider a molecular system with a ground electronic state strongly coupled to a single primary nuclear coordinate Q. The Hamiltonian of the system is

$$H_S = \frac{P^2}{2M} + U(Q) \tag{2.1}$$

where P is the conjugate momentum of Q. The molecular system is interacting with an off-resonant laser field, $E(\boldsymbol{r},t)$, where $\boldsymbol{r}$ is the position of the

molecular system. We consider the 3rd- and 5th-order off-resonant experiments. The system first interacts with N pair of pulses for the $2N+1$th order optical process, which have the same time profile $E_j(t)$ ($j=1$ and 2), but different wave vectors $\boldsymbol{k}_j$ and $\boldsymbol{k}'_j$ and frequencies Ω_j and Ω'_j for the jth pair of pulse, respectively. The last pulse $(\boldsymbol{k}_T, \Omega_T)$ is the probe that generates the signal. The pulse configuration of the 5th order experiment is given in Fig. 1. The effective Hamiltonian including laser interaction is then given by [22,23]

$$H_{\rm eff} = H_{\rm S} - E^2(\boldsymbol{r},t)\,\alpha(Q) \tag{2.2}$$

where $\alpha(Q)$ is the coordinate dependent polarizability. The physical observable in optical experiments is the polarization. The third-order and the fifth-order polarization are, respectively, expressed as [1]

$$\begin{aligned} P^{(3)}(t) = {} & 2\int_0^\infty {\rm d}\tau_1 E_T(t) E_1^2(t-\tau_1) \\ & \times \exp(i\Omega_T t - i\boldsymbol{k}_T\boldsymbol{r}) \\ & \times \left[\cos(\Delta\Omega_1(t-\tau_1) - \Delta\boldsymbol{k}_1\boldsymbol{r}) + 1\right] \\ & \times R^{(3)}(\tau_1) \end{aligned} \tag{2.3}$$

and

$$\begin{aligned} P^{(5)}(t) = {} & 2^2\int_0^\infty {\rm d}\tau_2 \int_0^\infty {\rm d}\tau_1 E_T(t) E_2^2(t-\tau_2) \\ & \times E_1^2(t-\tau_2-\tau_1)\exp(i\Omega_T t - i\boldsymbol{k}_T\boldsymbol{r}) \\ & \times \left[\cos(\Delta\Omega_2(t-\tau_2) - \Delta\boldsymbol{k}_2\boldsymbol{r}) + 1\right] \\ & \times \left[\cos(\Delta\Omega_1(t-\tau_2-\tau_1) - \Delta\boldsymbol{k}_1\boldsymbol{r}) + 1\right] \\ & \times R^{(5)}(\tau_2,\tau_1) \end{aligned} \tag{2.4}$$

where $\Delta\boldsymbol{k}_j \equiv \boldsymbol{k}_j - \boldsymbol{k}'_j$, $\Delta\Omega_j \equiv \Omega_j - \Omega'_j$. The third- and the fifth-order response functions are defined by

$$R^{(3)}(\tau_1) = \frac{i}{\hbar} tr\{[\alpha(\tau_1), \alpha(0)]\,\rho_g\} \tag{2.5}$$

$$\begin{aligned} R^{(5)}(\tau_2,\tau_1) = {} & -\frac{1}{\hbar^2} tr\{[[\alpha(\tau_1+\tau_2), \alpha(\tau_1)], \alpha(0)]\,\rho_g\} \end{aligned} \tag{2.6}$$

Here, ρ_g is the equilibrium distribution

$$\rho_g = \exp[-\beta H_{\rm S}]/tr\{\exp[-\beta H_{\rm S}]\} \tag{2.7}$$

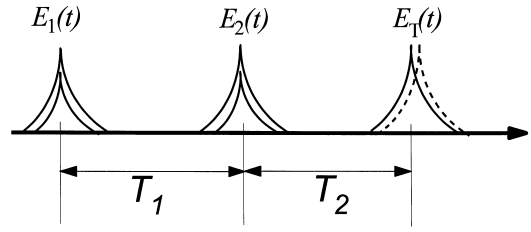

Fig. 1. Pulse configuration for the fifth-order experiment. The system first interacts with two pairs of pulses, which have the same time profile $E_j(t)$, but different wave vectors $\boldsymbol{k}_j$ and $\boldsymbol{k}'_j$ and frequencies Ω_j and Ω'_j for the jth pair of pulse ($j=1$ and 2), respectively. The last pulse $(\boldsymbol{k}_T,\ \Omega_T)$ is the probe that generates the signal.

and $\alpha(\tau)$ represents

$$\alpha(\tau) \equiv \exp\left(\frac{i}{\hbar}H_{\rm S}\tau\right)\alpha(Q)\exp\left(-\frac{i}{\hbar}H_{\rm S}\tau\right) \tag{2.8}$$

The response function can be rewritten as

$$\begin{aligned} R^{(3)}(\tau_1) &= \frac{i}{\hbar} tr\left\{\alpha(\tau_1)\left(\alpha^\times(0)\,\rho_g\right)\right\} \\ &= \frac{i}{\hbar} tr\left\{\alpha e^{-\frac{i}{\hbar}H_{\rm S}\tau_1}\left(\alpha^\times\rho_g\right)e^{\frac{i}{\hbar}H_{\rm S}\tau_1}\right\} \end{aligned} \tag{2.9}$$

$$\begin{aligned} & R^{(5)}(\tau_2,\tau_1) \\ & = -\frac{1}{\hbar^2} tr\left\{\alpha(\tau_1+\tau_2)\left[\alpha^\times(\tau_1)\left(\alpha^\times(0)\,\rho_g\right)\right]\right\} \\ & = -\frac{1}{\hbar^2} \\ & \quad \times tr\left\{\alpha e^{-\frac{i}{\hbar}H_{\rm S}\tau_2}\left[\alpha^\times\left(e^{-\frac{i}{\hbar}H_{\rm S}\tau_1}\left(\alpha^\times\rho_g\right)e^{\frac{i}{\hbar}H_{\rm S}\tau_1}\right)\right]\right. \\ & \quad \left.\times e^{\frac{i}{\hbar}H_{\rm S}(\tau_2)}\right\} \end{aligned} \tag{2.10}$$

where $A^\times B \equiv AB - BA$. Eq. (2.10) describes the following time evolution of the density matrix element: (i) Initially, the system is in the equilibrium state, $\rho_{\rm g}$. The polarization operator attached with the first pair of laser pulses, $\alpha^\times$, then operates upon ρ_g. This sets the time $t=0$. (ii) The density matrix obtained by (i) then evolves in time from $t=0$ to $t=\tau_1$ following the time evolution operator of the system, i.e., $\rho(\tau_1) = \exp[-iH_S\tau_1/\hbar](\alpha^\times\rho_g)\exp[iH_S\tau_1/\hbar]$. (iii) At time $t=\tau_1$ the polarization operator attached with the second pair of laser pulses,

$\alpha^{\times}$, operates upon the density matrix, $\rho(\tau_1)$, which is obtained by (ii). (iv) After the second pair of laser interaction, the density matrix then evolves in time from $t=\tau_1$ to $t=\tau_2$, following the time evolution operator, i.e., $\rho'(\tau_2,\ \tau_1)=\exp[-iH_S\tau_2/\hbar][\alpha^{\times}\rho(\tau_1)]\exp[iH_S\tau_2/\hbar]$. (v) The polarization operator of the last laser pulse, α, then operates upon the density matrix calculated by (iv). (vi) Tracing over all degrees of freedom reduces the response function given by Eq. (2.10), i.e., $R^{(5)}(\tau_2,\ \tau_1)=\mathrm{tr}\{\alpha\rho(\tau_1+\tau_2)\}/\hbar^2$. A representative calculation for the Morse potential will be presented in Section 4. Note that the time evolution of the third-order signal, Eq. (2.9), corresponds to the steps (i), (ii), (v) and (vi).

The time evolution of the density matrix can be evaluated by integrating the quantum Liouville equation,

$$\dot{\rho}(t)=-\frac{i}{\hbar}[\,\rho(t),H_s] \tag{2.11}$$

For example, the density matrix elements described by step (ii) can be calculated by integrating Eq. (2.11) from $t=0$ to τ_1 with the initial condition $(\alpha^{\times}\rho_g)$. Similarly the density matrix elements described by step (iv) can be calculated by integrating Eq. (2.11) from $t=\tau_1$ to $\tau_1+\tau_2$ with the initial condition $[\alpha^{\times}\rho(\tau_1)]$. One can apply the above prescription of calculating response functions to any kind of system, if one knows the polarization operator and the equation of motion for the density matrix. In the following, we evaluate the third and fifth-order response function using the quantum Fokker–Planck equation instead of the Liouville Equation (Eq. (2.11)).

3. Quantum Fokker–Plank equation for a Gaussian–white noise

We assume that the primary nuclear coordinate is coupled to a bath which is represented by a set of harmonic oscillators with frequencies ω_n, masses m_n, coordinate x_n, and momenta p_n. The interaction between the primary nuclear coordinate and the nth bath oscillator is assumed to be linear with a coupling strength c_n. The total Hamiltonian is then given by

$$H=H_{\mathrm{S}}+\sum_n\left[\frac{p_n^2}{2m_n}+\frac{m_n\omega_n^2}{2}\left(x_n-\frac{c_nQ}{m_n\omega_n^2}\right)^2\right] \tag{3.1}$$

All information about the bath, which is required for the reduced description of the system dynamics, is contained in its initial temperature and its spectral density

$$J(\omega)\equiv\omega\sum_n\left(\frac{c_n^2}{4m_n\omega_n^2}\right)(\delta(\omega-\omega_n)+\delta(\omega+\omega_n)) \tag{3.2}$$

The function $J(\omega)$ is related to the symmetric correlation function of a collective bath coordinate ($X=\sum c_nx_n$) [16],

$$\frac{1}{2}\langle X(t)X+XX(t)\rangle=\hbar\int\mathrm{d}\omega\,J(\omega)\coth\left(\frac{\beta\hbar\omega}{2}\right)\cos(\omega t) \tag{3.3}$$

where $\beta=1/k_{\mathrm{B}}T$ is the inverse temperature of the bath, and the time evolution of X is determined by the bath Hamiltonian. If the spectral distribution is given by $J(\omega)=M\zeta\omega/2\pi$ (the Ohmic distribution) and the bath temperature is high (i.e., $\coth(\beta\hbar\omega/2)\approx 2/\beta\hbar\omega$), we have $\frac{1}{2}\langle X(t)X+XX(t)\rangle=2M\zeta\delta(t)/\beta$. This correlation function corresponds to the Gaussian–white noise. In this case, we can obtain an equation of motion for the reduced system density matrix, $\rho(Q,Q';t)=tr_{\mathrm{B}}\{|Q,\boldsymbol{x}\rangle\langle Q',\ \boldsymbol{x}'|\}$ (the quantum master equation). In the Wigner (phase space) representation [17]

$$W(P,R;t)\equiv\frac{1}{2\pi\hbar}\int_{-\infty}^{\infty}\mathrm{d}r e^{iPr/\hbar}\times\rho(R-r/2,R+r/2;t) \tag{3.4}$$

the equation of motion (the quantum Fokker–Planck equation) is expressed as

$$\frac{\partial}{\partial t}W=-\mathscr{L}_{\mathrm{S}}W+\Gamma W \tag{3.5}$$

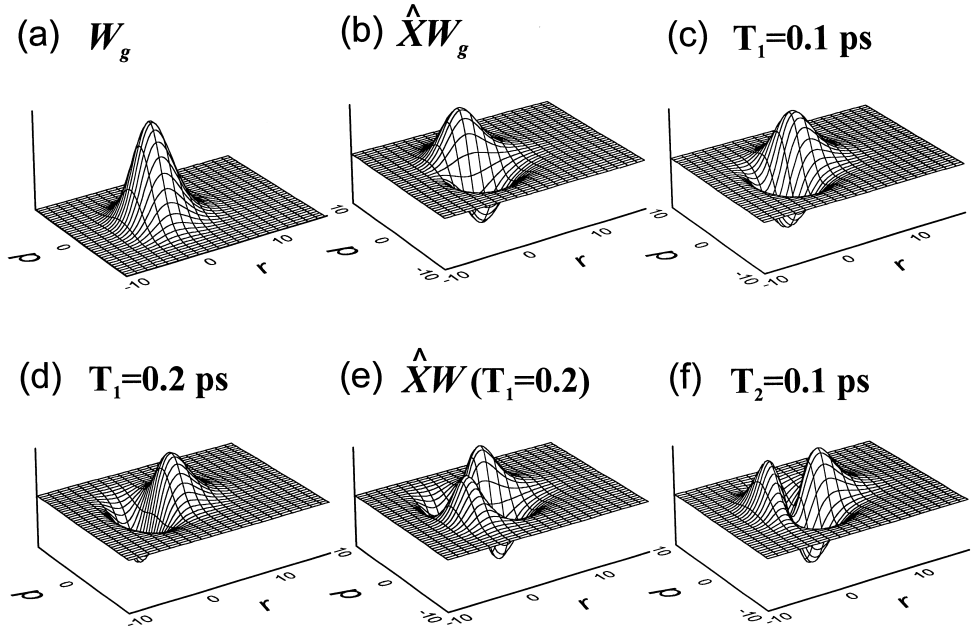

Fig. 2. The time-evolution of the wave packet in the fifth-order response function.

Here, [24],

$$-\mathscr{L}_S W \equiv -\frac{P}{M}\frac{\partial}{\partial R}W(P,R;t) - \frac{1}{\hbar}\int\frac{dP'}{2\pi\hbar}V(P-P',R)W(P',R;t) \tag{3.6}$$

with

$$V(P,R) = 2\int_{-\infty}^{\infty} dr\,\sin\left(\frac{Pr}{\hbar}\right) \times\left[U\left(\frac{R+r}{2}\right) - U\left(\frac{R-r}{2}\right)\right] \tag{3.7}$$

and the Ornstein–Uhlenbeck operator which describes Brownian motion in momentum space is

$$\Gamma \equiv \zeta\frac{\partial}{\partial P}\left(P + \frac{M}{\beta}\frac{\partial}{\partial P}\right) \tag{3.8}$$

In the Wigner representation, the polarization operators are expressed as

$$\alpha(Q)\rho \to \hat{A}W \equiv \int\frac{dP'}{2\pi\hbar}A(P-P',R)W(P',R;t)$$
$$\frac{i}{\hbar}\alpha^{\times}(Q)\rho \to \hat{X}W \equiv \frac{1}{\hbar}\int\frac{dP'}{2\pi\hbar}X(P-P',R) \times W(P',R;t) \tag{3.9}$$

where

$$A(P,R) = i\int_{-\infty}^{\infty} dr\,\exp(iPr/\hbar)\,\alpha(R-r/2)$$
$$X(P,R) = 2\int_{-\infty}^{\infty} dr\,\sin(Pr/\hbar) \times\left[\alpha(R-r/2) - \alpha(R+r/2)\right] \tag{3.10}$$

Notice that the quantum Fokker–Planck equation for a Gaussian–white noise bath can be applied only for the high temperature system, i.e., $\hbar\omega_c/k_B T \ll 1$, where ω_c is the characteristic frequency of the system, since to obtain Eq. (3.8) we have made the high temperature approximation $\coth(\beta\hbar\omega_c/2) \approx 2/\beta\hbar\omega_c$. In the case of a harmonic potential system, the quantum Fokker–Planck equation coincides with the classical one, however, in the low temperature case, the 'quantum results' obtained from this equation differ from the exact results obtained from the path integral approach [25]. In the flowing analysis, the temperatures are chosen to satisfy this limitation. If one applies the equation beyond this limitation, then one obtains nonphysical results such as the negative probability of density matrix elements, which is known as breaking of dynamic positivity [26]. This limitation can be reduced if one uses the quantum Fokker–Planck equation for a Gaussian–Markovian bath [18,19,21].

It is now straightforward to specialize Eqs. (2.9) and (2.10) to the Fokker–Planck equation. The response functions are then expresses as

$$R^{(3)}(\tau_1) = tr\left\{ \hat{A}\exp\left[-(\mathscr{L}_S - \Gamma)\tau_1\right]\hat{X}W_g \right\} \quad (3.11)$$

$$R^{(5)}(\tau_2,\tau_1) = tr\left\{ \hat{A}\exp\left[-(\mathscr{L}_S - \Gamma)\tau_2\right]\hat{X} \times \exp\left[-(\mathscr{L}_S - \Gamma)\tau_1\right]\hat{X}W_g \right\} \quad (3.12)$$

where W_g is the equilibrium distribution function in the Wigner representation. This can be obtained by integrating the Fokker–Planck equation (Eq. (3.6)) with same temporally initial condition, such as $W(P,Q) = \exp[-\beta H_S(P,Q)]$, since if one integrates the equation of motion long enough, the distribution reaches to the 'true' quantum equilibrium distribution. We then calculate the third- and fifth-order signal as described by the steps (i)–(vi) in Section 2 using the quantum Fokker–Planck equation (Eq. (3.6)). Note that the trace operation in Eqs. (3.11) and (3.12) corresponds to the integration over P and Q.

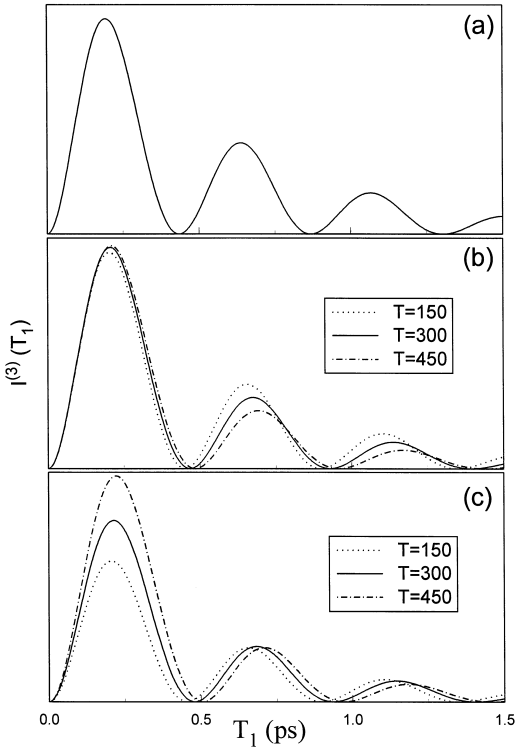

Fig. 3. The third-order signal $I^{(3)}(T_1)$ for (a) the harmonic potential with the linear polarizability ($\alpha(q) = \alpha_1 q$); (b) the Morse potential with the linear polarizability ($\alpha(q) = \alpha_1 q$); (c) the Morse potential with nonlinear polarizability ($\alpha(q) = \alpha_1 q + \alpha_2 q^2$) in the weak damping case. Here, we used the arbitrary unit for $I^{(3)}$. In cases (b) and (c), we calculated the signals for the different temperatures ($T = 150$, 300, and 450 K). The signal in case (a) is temperature independent and we show only one example.

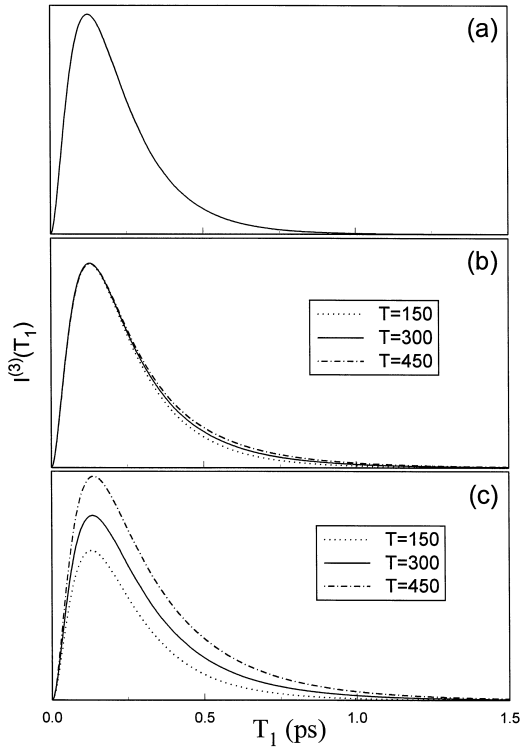

Fig. 4. The third-order signal $I^{(3)}(T_1)$ for (a) the harmonic potential with the linear polarizability; (b) the Morse potential with the linear polarizability; (c) the Morse potential with nonlinear polarizability in the strong damping case. The parameters are the same as in Fig. 3 except the damping constant.

In Section 4, we calculate the 3rd and 5th order response function for a Morse potential system.

4. Numerical calculations of the third- and fifth-order off-resonant signals

In the impulsive limit the pulse envelope can be approximated by $E_T(t) = \delta(t - T_1)$ and $E_1(t) = \delta(t)$ for the 3rd order, and $E_T(t) = \delta(t - T_1 - T_2)$, $E_1(t) = \delta(t)$, and $E_2(t) = \delta(t - T_1)$ for the 5th order (see

Fig. 1). Then we can perform the time integrations over τ_j and the total signal intensity which is related to the square of the polarization, is given by (up to a proportionality constant)

$$I^{(3)}(T_1) = |R^{(3)}(T_1)|^2 \tag{4.1}$$

The 5th order signal is given by

$$I^{(5)}(T_1,T_2) = |R^{(5)}(T_2,T_1)|^2 \tag{4.2}$$

In the following, we calculate the 3rd and 5th order signals for a Morse potential surface expressed as

$$U(Q) = E_e\{1 - e^{-aQ}\}^2 \tag{4.3}$$

where E_e and a are the dissociation energy and the curvature of the potential, respectively. Hereafter, we employed the dimensionless coordinate and momentum defined by $q \equiv Q\sqrt{M\omega_0/\hbar}$ and $p \equiv P\sqrt{1/M\hbar\omega_0}$, respectively, where $\omega_0 \equiv \sqrt{U''(Q)/M}$. The curvature of the potential, a, is also measured in this unit. We set $E_e = 3649.5$ cm^{-1}, $a = 0.6361$ as the ground state of the Cs_2 molecule [27,28]. The fundamental frequency is then given by $\omega_0 = 38.7$ cm^{-1}. Note that we did not specify M, since it does not play any role in this dimensionless unit. The polarizability is assumed to be

$$\alpha(q) \equiv \alpha_1 q + \alpha_2 q^2 \tag{4.4}$$

and we consider two special cases of linear ($\alpha_1 = 1$ and $\alpha_2 = 0$) and the nonlinear polarizability ($\alpha_1 = 1$ and $\alpha_2 = 0.05$). As a reference, we also calculated signals for a harmonic potential surface defined by

$$U(q) = \frac{1}{2}\hbar\omega_0 q^2 \tag{4.5}$$

In the harmonic case, the 3rd and the 5th order response functions in the lowest order of α are

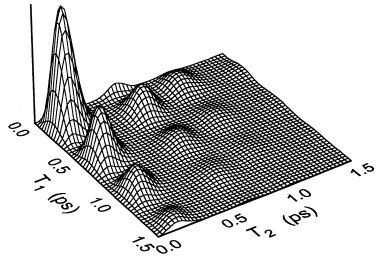

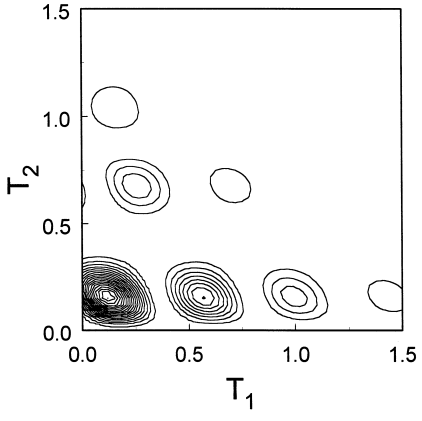

Fig. 5. The 2D signal $I^{(5)}(T_1,T_2)$ for the harmonic potential with nonlinear polarizability ($\alpha(q) = \alpha_1 q + \alpha_2 q^2$) in the weak damping case. In this harmonic case, the signals are temperature independent. The upper figure shows the profile of the signal, whereas the lower one shows its counter plot. Here, we used the arbitrary unit for $I^{(5)}$. Note that the signal in this case is temperature independent.

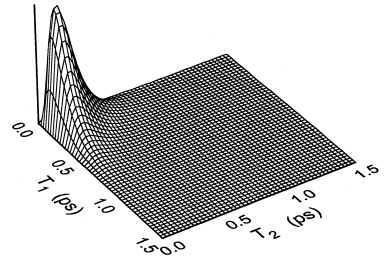

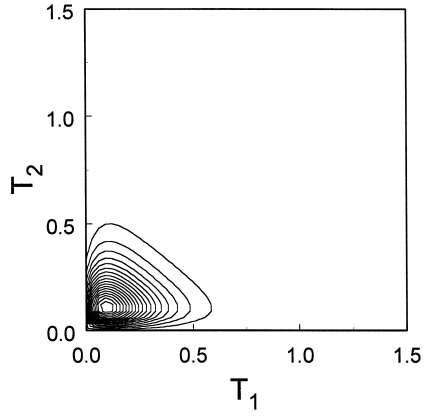

Fig. 6. The 2D signal $I^{(5)}(T_1,T_2)$ for the harmonic potential with nonlinear polarizability ($\alpha(q) = \alpha_1 q + \alpha_2 q^2$) in the strong damping case. Note that the signal in this case is temperature independent.

analytically calculated for the Gaussian–white noise case as [1]

$$R^{(3)}(\tau_1) = \frac{2i\alpha_1^2}{\hbar} D^{(-+)}(\tau_1) \tag{4.6}$$

$$R^{(5)}(\tau_2,\tau_1) = \frac{4}{\hbar^2}\alpha_1^2\alpha_2 D^{(-+)}(\tau_2) \times \left[D^{(-+)}(\tau_1) + D^{(-+)}(\tau_1+\tau_2) \right] \tag{4.7}$$

where

$$D^{-+}(t) \equiv \frac{\omega_0}{\Omega}\exp(-\zeta t/2)\sin(\Omega t) \tag{4.8}$$

with $\Omega \equiv \sqrt{\omega_0^2 - \gamma^2/4}$. We should notice that, in this harmonic case, both the 3rd and 5th order signals do not depend on the temperature. In addition, the lowest order contribution of the 5th order signals start from $\alpha_1^2\alpha_2$ not from α_1^3 as mentioned before.

In the following, we use two values of friction $\zeta = 10\ \mathrm{cm}^{-1}$ (weak) and $\zeta = 100\ \mathrm{cm}^{-1}$ (strong) and three values of temperature $T = 150$, 300, and 450 K all of which satisfy the condition, $2\pi\hbar\omega_0/k_BT \ll 1$.

The numerical integrations of the Fokker–Planck equations were performed by using second order Runge–Kutta method for finite difference expressions of the momentum and the coordinate space. The size of mesh was chosen to be 80×400 in the mesh range $-10 < p < 10$ and $-10 < q < 18$. On the mesh, the kinetic operator $p\partial W/\partial r$ was approximated by a left-hand difference, $p_i(W(p_i,q_j) - W(p_i,q_{j-1}))/\Delta r$ for $p_i > 0$ and by a right-hand difference $p_i(W(p_i,q_{j+1}) - W(p_i,q_j))/\Delta q$ for $p_i < 0$. The discrete Fourier expression was used for the potential kernel Eq. (3.6). The accuracy of the calculations had been checked by changing the mesh size. For a harmonic case, we compared the present numerical results to the analytical result given in Eq.

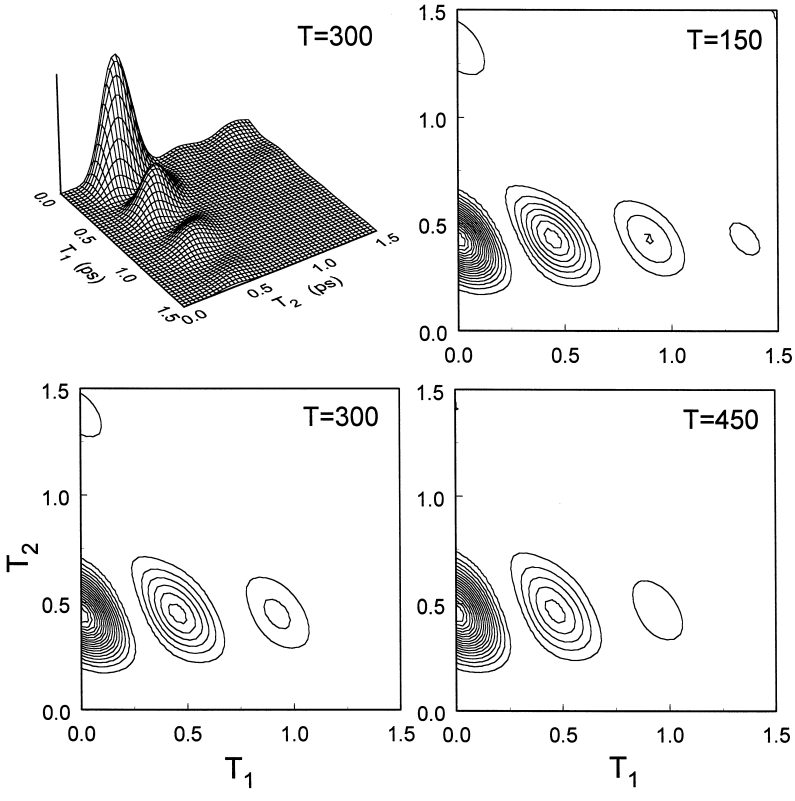

Fig. 7. The 2D signal $I^{(5)}(T_1,T_2)$ for the Morse potential with the linear polarizability ($\alpha(q) = \alpha_1 q$) in the weak damping case. We calculated signals for three different temperatures ($T = 150$, 300, and 450 K) and displayed as the counter plots.

(4.6) and verified the results. We then calculated the 3rd and 5th order signals by integrating the Fokker–Planck equation following the steps shown in Section 2.

First, we present the time-evolution of wave packets during the different propagation periods. Here, we consider the weak damping case with linear polarizability. Fig. 2a depicts the equilibrium Wigner distribution, $W_g(p,q)$, calculated from Eq. (3.5). To obtain this, we set the temporary initial condition, $W(p,q;t_i) = \exp[-\beta\omega(p^2 + U(q)]$, and integrate the equation of motion from $t = -1$ to 0 ps so that the distribution attains to the steady state. Fig. 2b shows the distribution after the operator $\alpha^{\times}$ operated on W_g, i.e., $W(\tau_1 = 0) = XW_g$. The wave packet, $W(\tau_1)$, then time evolves and rotates in the phase space as shown in Fig. 2c and d. At time $\tau = 2$ ps, a second pair of laser pulses interacts with the distribution function. The distribution $W'(\tau_1,\ \tau_2 = 0) = \hat{X}W(\tau_1)$ is displayed in Fig. 2e. The excited wave packet then rotates in the phase space as shown in Fig. 2f. The fifth-order signal can be calculated from $AW(\tau_2)$ by integrating over q and p. Note that the time-evolution of the wave packet in the third-order response function from time $\tau = 0$ to 2 ps corresponds to Fig. 2a–d.

4.1. Third-order signal

Figs. 3 and 4 present the 3rd order signal for (a) the harmonic potential with linear polarizability ($\alpha(q) = \alpha_1 q$), (b) the Morse potential with linear polarizability ($\alpha(q) = \alpha_1 q$), and (c) the Morse potential with nonlinear polarizability ($\alpha(q) = \alpha_1 q + \alpha_2 q^2$) for different temperatures ($T = 150$, 300, and 450 K). Here, we set $\alpha_2 = 0.05\alpha_1$. In case (a), the signal is temperature independent and we show the figure at $T = 300$ K only. In cases (b) and (c), all peaks shift to longer times as the temperature is increased. In cases (b) and (c), the oscillation period

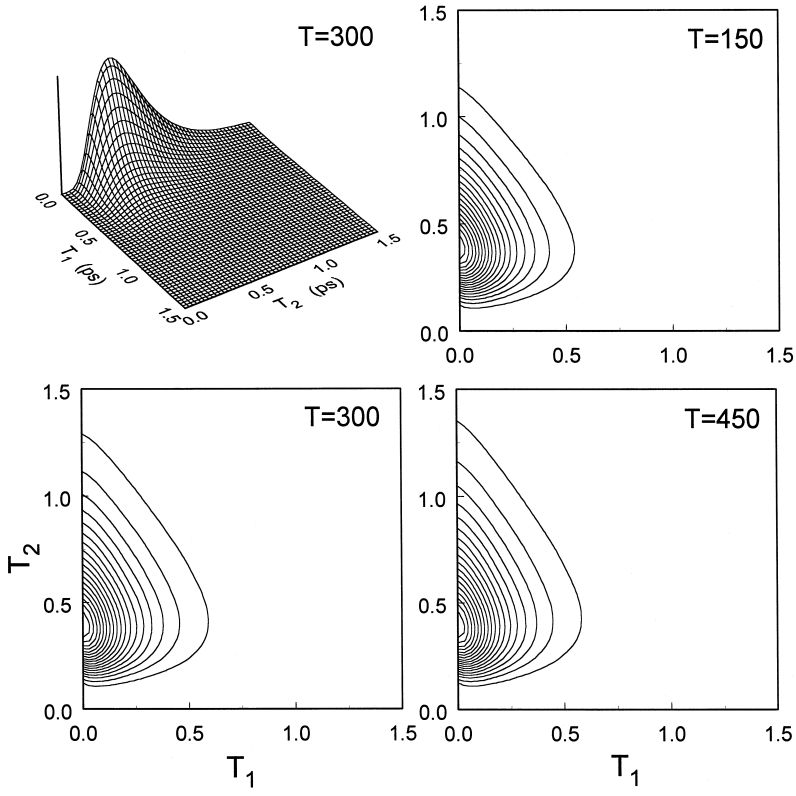

Fig. 8. The 2D signal $I^{(5)}(T_1,T_2)$ for the Morse potential with the linear polarizability ($\alpha(q) = \alpha_1 q$) in the strong damping case.

becomes longer as the temperature is increased. In the Morse potential, the energy between adjacent levels decreases with increasing quantum number. At higher temperature more levels become populated, showing up in a smaller effective frequency.

The temperature dependence in cases (b) and (c) is, however, quite different. In the linear polarizability case (b), the peak height around $T = 0.2$ does not depend on temperature, while the heights of the second and third peak around $T = 0.65$ and 1.1 ps, respectively, decay faster when the temperature is higher. This is because the transition frequencies between vibrational levels are not the same in the Morse potential system and, at high temperatures, the contribution of higher levels, which have longer vibrational periods, become important.

Fig. 3c shows the nonlinear case. In addition to $\langle[Q(t),Q(0)]\rangle$, we have the contribution from $\langle[Q(t),Q^2(0)]\rangle$, $\langle[Q^2(t),Q(0)]\rangle$, etc. Then, the peaks are higher than those of Fig. 2b. If the temperature is low, however, the distribution function is well localized at the bottom of the potential, so that we have $Q^2W \ll QW$. Therefore, the contribution from $\langle[Q^2(t),Q(0)]\rangle$, etc. can be neglected at low temperatures, and the signal approaches to the harmonic one.

Fig. 4 shows the strong damping case. Because of the overdamped motion of the wave packet, the signal decays monochromatically. In case (b), we observe a small peak shift with changing of temperature. In case (c), the heights of peaks also change as discussed above. In any case, however, the differences between the harmonic and Morse potential are very small and it is impossible to determine the shape of the potential based on the third-order experiments.

4.2. Fifth-order signal

Next, we present the fifth-order off-resonant 2D signals for different couplings and temperatures as a

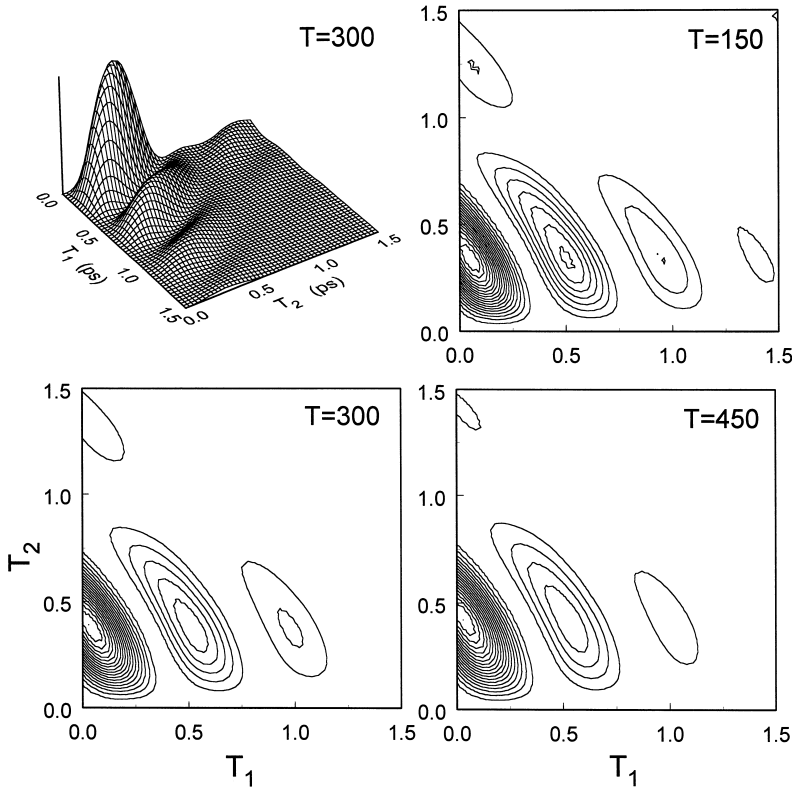

Fig. 9. The 2D signal $I^{(5)}(T_1,T_2)$ for the Morse potential with nonlinear polarizability ($\alpha(q) = \alpha_1 q + \alpha_2 q^2$) in the weak damping case.

function of time. First we discuss the signal for the harmonic potential with nonlinear polarizability $\alpha(q) = \alpha_1 q + \alpha_2 q^2$ in the cases of weak and strong damping (Figs. 5 and 6). As seen from Eq. (4.7), the signal of the harmonic system is temperature independent, therefore we present the case $T = 300$ K only. In Fig. 5, we observe the coherent oscillation with the frequency $2\omega_0$ in T_1 directions as was shown in Ref. [10]. As seen from the analytical expression Eq. (4.7) with Eq. (4.8), the decay rate of peaks in T_1 direction is $-\zeta$, whereas in the T_2 direction consists of three components with the decay rates $-\zeta$, -2ζ, and $-3/2\zeta$, respectively. Thus, the decay in T_2 direction is faster than T_1 direction. In the overdamped case, Fig. 5, the signal decays mono chromatically. As observed in the weak damping case, the decay rate in T_1 direction is larger than that in T_2.

Figs. 7 and 8 show the 2D signals for the Morse potential with linear polarizability $\alpha(Q) = \alpha_1 Q$. Due to the anharmonicity, we observe the signal in the lowest order (α_1^3). In fifth-order, anharmonicity is the essential source of the signal, whereas in third-order, it gives only a minor correction to the signal. Thereby, the profile of the signal is very different from that of the harmonic case.

Fig. 7 shows the signal for weak damping. Compared with the harmonic case, the peaks in this figure shift to longer T_2. The time period between the peaks in T_2 direction is also changed. Such features had been found in the analysis of a system with weak anharmonicity [10]. Our results are similar especially in the low temperature case, where the initial distribution of the wave packet is localized in the bottom of the potential and the Morse potential can be approximated by a harmonic potential with weak anharmonicity. We should notice, however, that the previous results for a system with weak anharmonicity are temperature independent, since the calculations were done by assuming very weak an-

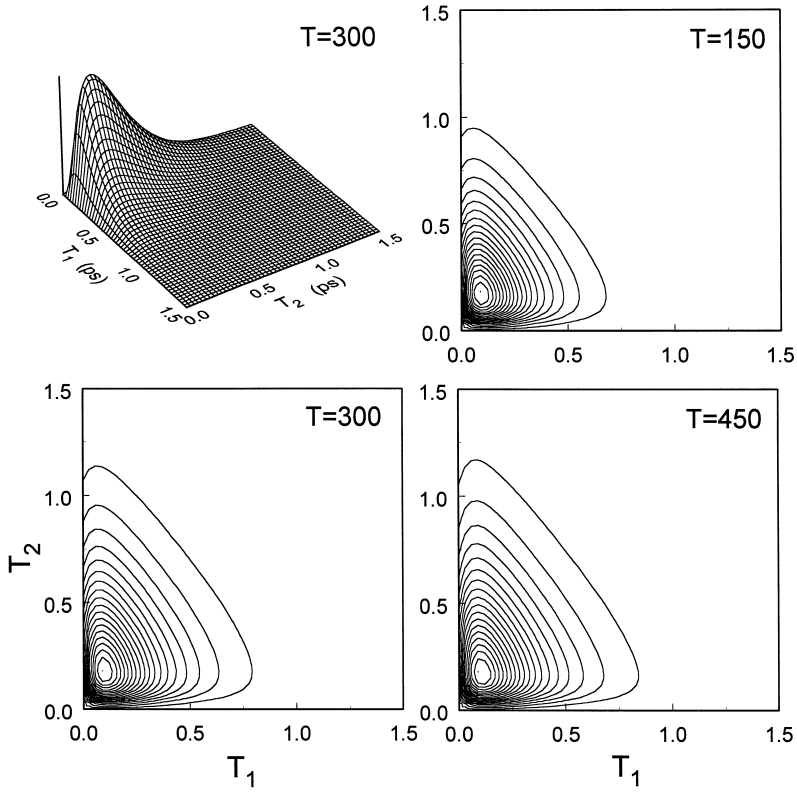

Fig. 10. The 2D signal $I^{(5)}(T_1,T_2)$ for the Morse potential with nonlinear polarizability ($\alpha(q) = \alpha_1 q + \alpha_2 q^2$) in the strong damping case.

harmonicity. In the present case, we employed the Morse potential in which the anharmonicity is very strong, and hence the profiles of the signals strongly depend on temperature. As seen in Fig. 7, the distances between the peaks become larger with increasing temperature. This is because the transition frequencies between vibrational levels become smaller at higher levels and they play major roles at high temperatures as discussed in the third-order case. This phenomenon is especially seen in the T_2 direction. The enhanced decay of the signal with increasing temperature is due to the beating between different transition frequencies.

Fig. 8 is for the strong damping case. The main difference from the harmonic case is the longer decay rate in the T_2 direction, which was also observed in Ref. [10]. The dependence of the temperature is smaller, since the coherent oscillations with different oscillation periods cannot play a role in this strong damping case.

Figs. 9 and 10 show these result for the nonlinear polarizability case. In addition to the contribution $\langle[[Q(t),Q(t')],Q(0)]\rangle$, in which the anharmonicity plays a major role, here, we have the contribution from $\langle[[Q(t),Q^2(t')],Q(0)]\rangle$, etc., in which the nonlinearity of the polarizability is the source of the signal. The obtained signal then shows mixed character of Figs. 5 and 7, and the peaks are spread out at the positions of peaks appeared in both Figs. 5 and 7. This mixed character can be observed not only in the weak damping case of Fig. 9, but also in the strong damping case of Fig. 10.

In any case, the differences between Figs. 5–10 are very large and one can easily identify the shape of the potential and the form of the polarizability even in the strong damping case.

5. Conclusion

In this paper, a theory was presented to study the dynamics of molecular systems with arbitrary potential by femtosecond third- and fifth-order Raman experiments. Our approach makes use of the quantum Fokker–Planck equation, which describes the quantum dynamics of a molecular system coupled to a Gaussian–white noise bath. We presented a rigorous procedure for calculating the third and fifth-order off-resonant signals, which can be used for any kind of kinetic equation. Then, we calculated the signals for (a) the harmonic case; (b) the Morse potential with linear polarizability case, and (c) the Morse potential with nonlinear polarizability for different temperatures and different coupling strengths. We show that, in contrast to the third-order experiments, the signals in fifth-order are very sensitive to the shape of potential and the coordinate dependence of the polarizability. In the Morse potential case, the temperature dependence of the signal, which could not be observed from the previous perturbative analysis, was studied. This temperature dependence arises because the transition frequencies in the higher vibrational levels, which have shorter oscillation periods, play a major role at high temperatures.

Although, we discuss here the Morse potential system only, our approach can be applied to systems with any shape of the potential. For instance, the applied Fokker–Planck approach allows us to study a potential system in trigonometric form with periodical boundary condition. It is also possible to calculate the fifth-order signal for a double well potential system where tunneling is important. By taking an advantage of the development of high speed work stations, we may study multi modes system described by a multidimensional potential surface. We leave them for future studies.

Acknowledgements

Financial support for this work was partially provided by Grand-in-Aid for Scientific Research from the Japan Ministry of Education, Science, Sports, and Culture.

References

[1] Y. Tanimura, S. Mukamel, J. Chem. Phys. 99 (1993) 9496.
[2] R.F. Loring, S. Mukamel, J. Chem. Phys. 83 (1985) 2116.
[3] S. Palese, J.T. Buontempo, L. Schilling, W.T. Lotshaw, Y. Tanimura, S. Mukamel, R.J.D. Miller, J. Phys. Chem. 98 (1994) 12466.
[4] K. Tominaga, K. Yoshihara, Phys. Rev. Lett. 74 (1995) 3061; K. Tominaga, G.P. Keogh, Y. Naitoh, K. Yoshihara, J. Raman Spec. 26 (1995) 495; K. Tominaga, K. Yoshihara, J. Chem. Phys. 104 (1996) 1159; J. Chem. Phys. 104 (1996) 4422.

[5] T. Steffen, K. Duppen, Phys. Rev. Lett. 76 (1996) 1224; T. Steffen, J.T. Fourkas, K. Duppen, J. Chem. Phys. 105 (1996) 7364; T. Steffen, K. Duppen, J. Chem. Phys. 106 (1997) 3854; Chem. Phys. Lett. 273 (1997) 47.
[6] A. Tokmakoff, J. Chem. Phys. 105 (1996) 13.
[7] A. Tokmakoff, G.R. Fleming, J. Chem. Phys. 106 (1997) 2569.
[8] A. Tokmakoff, M.J. Lang, D.S. Larsen, G.R. Fleming, Chem. Phys. Lett., in press.
[9] J.A. Leegwater, S. Mukamel, J. Phys. Chem. 102 (1995) 2365; V. Khidekel, S. Mukamel, Chem. Phys. Lett. 240 (1995) 304; V. Khidekel, S. Mukamel, Chem. Phys. Lett. 263 (1996) 350, Erratum; V. Khidekel, V. Chernyak, S. Mukamel, J. Chem. Phys. 105 (1996) 8543.
[10] K. Okumura, Y. Tanimura, J. Chem. Phys. 105 (1996) 7294; J. Chem. Phys. 107 (1997) 2267; Chem. Phys. Lett. 277 (1997) 159.
[11] K. Okumura, Y. Tanimura, Chem. Phys. Lett. 278 (1997) 175.
[12] S. Saito, I. Ohmine, J. Chem. Phys. 108 (1998) 240.
[13] R.L. Murry, J.T. Fourkas, J. Chem. Phys. 107 (1997) 9726.
[14] M. Cho, K. Okumura, Y. Tanimura, J. Chem. Phys. 108 (1998) 1326.
[15] R. Kubo, M. Toda, N. Hashitsume, Statistical Physics, Vol. 2, Springer-Verlag, Berlin, 1985.
[16] Y. Tanimura, R. Kubo, J. Phys. Soc. Jpn. 58 (1989) 101.
[17] A.O. Caldeira, A.J. Leggett, Physica 121A (1983) 587.
[18] Y. Tanimura, P.G. Wolynes, Phys. Rev. A 43 (1991) 4131.
[19] Y. Tanimura, P.G. Wolynes, J. Chem. Phys. 96 (1992) 8485.
[20] Y. Tanimura, S. Mukamel, J. Chem. Phys. 101 (1994) 3049.
[21] Y. Tanimura, Y. Maruyama, J. Chem. Phys. 107 (1997) 1779.
[22] R.W. Hallwarth, Prog. Quant. Electr. 5 (1977) 1.
[23] Y.J. Yan, S. Mukamel, J. Chem. Phys. 94 (1991) 997.
[24] W.R. Frensley, Rev. Mod. Phys. 62 (1990) 745.
[25] H. Grabert, P. Schramm, G.-L. Ingold, Phys. Rep. 168 (1988) 115.
[26] H. Spohn, Rev. Mod. Phys. 52 (1980) 569.
[27] M. Raab, G. Honing, W. Demeteröder, C.R. Vidal, J. Chem. Phys. 74 (1982) 4370.
[28] W. Weickenmeier, U. Diemer, M. Wahl, M. Raab, W. Demtröder, W. Müller, J. Chem. Phys. 82 (1985) 5354.